Supplementary Information

Role of Tin Seed Layers in SEI Evolution and Lithium Electrodeposition

Ewelina Wiśniewska[1,$ #], Xiaorui Shi[1, #], Rone Newitt[1], Ved Sanyal[2], Krishnaveni Palanisamy[1,3], Svetlana Menkin[1,3*]

1. Yusuf Hamied Department of Chemistry, University of Cambridge, Lensfield Road, Cambridge, CB2 1EW, UK.
2. School of Chemistry, University of Edinburgh, Edinburgh, EH9 3FJ, UK.
3. The Faraday Institution, Quad One, Harwell Science and Innovation Campus, Didcot, OX11 ORA, UK.

* Corresponding author email: sm2383@cam.ac.uk

# Equal contribution.

$ presenting author

Tested Conditions	Effect	Confirmed By
0.8 M Thiourea	Sn coating observed	XRD, EDX
1.6 M Thiourea	More Sn deposition, some Sn grains observed	EDX
60 s Deposition time	Sn coating observed	EDX
360 s Deposition time	More deposition	EDX
10 min Deposition time	More deposition	XRD, EDX
1 hour Deposition time	More deposition, large Sn grains observed	XRD, EDX
No pre-treatment	Sn coating observed	XRD
Acetic acid pre-treatment of Cu	No improvement	Cycling
Acetone pre-treatment of Cu	No improvement	Cycling

Table S1 *Coating conditions tested to obtain the best conditions for applying consistent coatings.*

1. A higher thiourea concentration in the coating bath led to more deposited Sn on the surface (Fig. S2). Sn grains were observed in the sample with 1.8 M thiourea concentration which may be similar to the Sn grains in the 1-hour coating samples used but this was not investigated here.
2. A longer coating time leads to more Sn deposition as you can fully form the intermetallic compound and the Sn layer on the surface with greater deposition times.
3. The effect of the pre-treatment on coatings was difficult to quantify as during galvanostatic cycling the discharge capacities were very similar between samples prepared by all pre-treatments and any difference between performance is easily explained by the inherent variability of coin cells produced. Pre-treatment was not investigated further.

Schematic of both plating methods used to coat samples on one side (Fig. S1). The floating method (left) involved filling a Viton O-ring with the bath solution until the liquid is filled above the height of the O-ring by surface tension. The foil is then floated on the bath solution taking care not to stick any part of the foil to the O-ring, which could prevent even coating. An alternative method (right) involved adding the bath solution dropwise onto the foil which should completely cover the Viton O-ring. This holds it above the platform, and the surface tension should hold the bath solution onto the foil after enough is added being careful not to add too much on leading to the solution spilling. In both methods it is possible to see clear tin coating formation beginning to occur after just 1 minute, however, the sample does not significantly change visually past this point despite more deposition occurring (Fig. 1).

During the washing stages care should be taken to change tweezers multiple times to ensure the entire surface is washed. It is also particularly easy to form permanent streaks on the sample surface when drying with N_2 so care should be taken to dry these as soon as possible. It is unclear what effect these streaks have on performance if any. The floating method was significantly easier to carry out in practice.

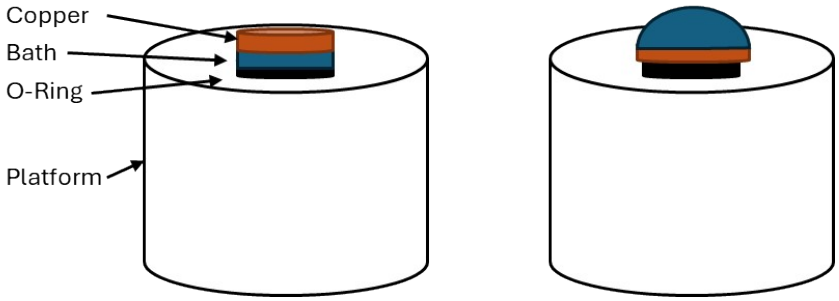

Comment []:

Figure S1 *Schematic of coating methods used during coating. Floating of a copper foil on the chemical bath solution (left) and dropping bath solution on top of foil (right)*

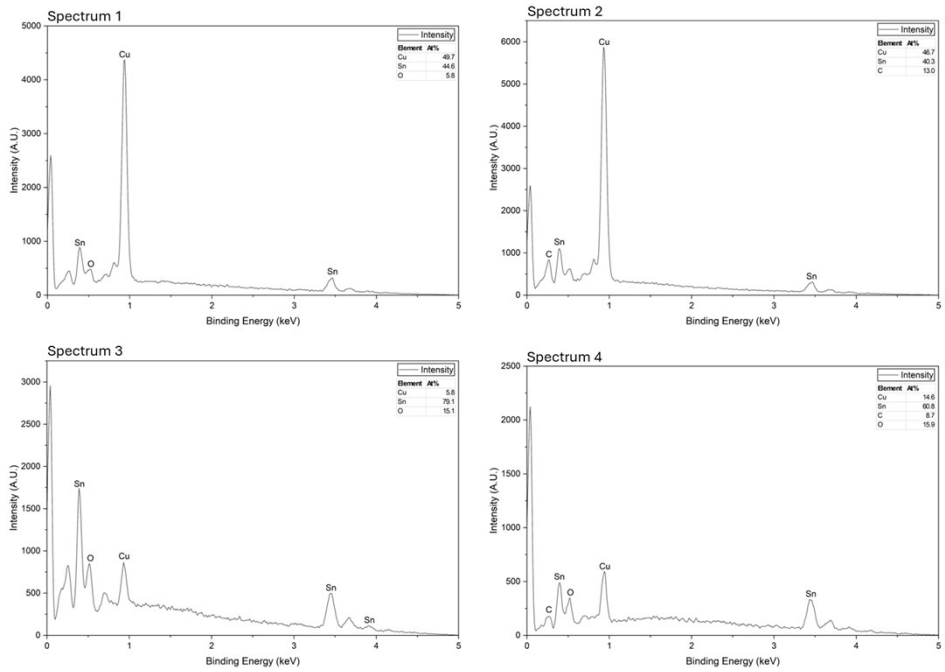

Fig S2a *EDX spectra of a fresh, 1-hour Sn@Cu coating corresponding to points 1, 2, 3 and 4 in Fig. S3.*

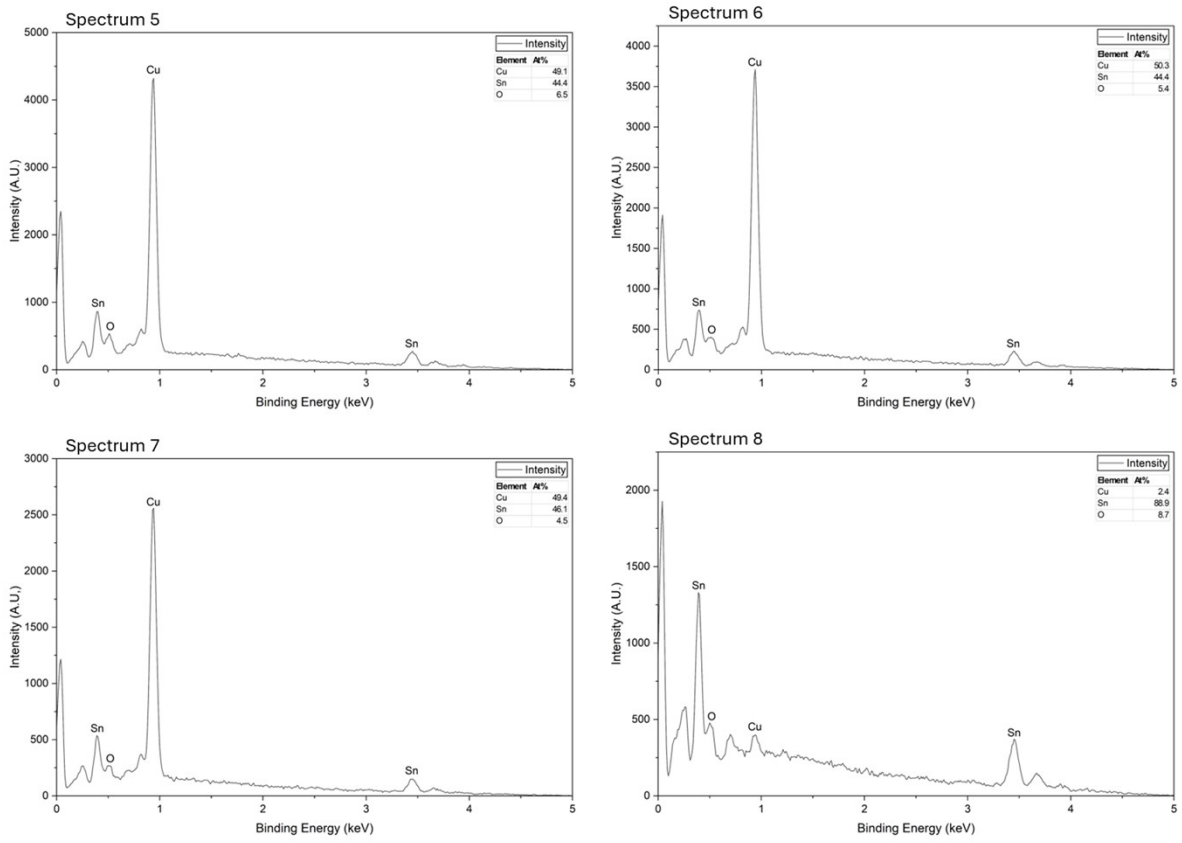

Fig S2b *EDX spectra of an aged, 1-hour Sn@Cu coating corresponding to points 5, 6, 7 and 8 in Fig. S3.*

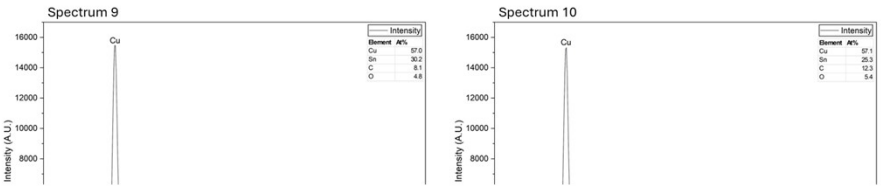

Fig S2c *EDX spectra of a fresh, 10-minute Sn@Cu coating corresponding to points 9, 10, 11, 12 and 13 in Fig. S3.*

Figure S3 *SEM images selected for EDX analysis; 10 min coating (left), fresh 1 h coating (centre) and aged 1 h coating (right)*

Comment []:

Comment []:

Comment []:

Sample	Spectrum	Copper At%	Tin At%	Cu:Sn ratio	Contaminants At%
10 Minute	9	57.0	30.2	65:35	4.8 O, 8.1 C
	10	57.1	25.3	69:31	5.4 O, 12.3 C
	11	50.7	34.5	60:40	5.9 O, 9.0 C
	12	59.5	31.5	65:35	9.1 C
	13	55.9	31.3	64:36	4.9 O, 7.8 C
Fresh 1 hour	1	49.7	44.6	53:47	5.8 O
	2	46.7	40.3	54:46	13.0 C
	3	5.8	79.1	7:93	15.1 O
	4	14.6	60.8	19:81	15.9 O, 8.7 C
Aged 1 hour	5	49.1	44.4	53:47	6.5 O
	6	50.3	44.4	53:47	5.4 O
	7	49.4	46.1	52:48	4.5 O
	8	2.4	88.9	3:97	8.7 O

Table S2 *EDX data of 10-minute coating, new 1-hour coating and an aged 1-hour coating.*

The bulk surface of the 1-hour coating shows a higher At% of Sn in the surface demonstrating that deposition continues to occur past ten minutes. The Cu:Sn ratio in both of the 1-hour samples shows bulk surface compositions of ~ 55:45 At%:At% which is the expected ratio in the Cu_6Sn_5 phase. Distinct tin grains are present in both 1-hour samples but absent in the 10-minute sample, supporting the assignment of the XRD data in Fig. 1. This indicates that once the equilibrium intermetallic composition is reached, additional tin deposition occurs as heterogeneous surface grains. In the 10 min sample, the grains are much less bright, consistent with the lower tin concentration.

Figure S4 Cyclic voltammetry measurements in a three-electrode configuration. **(a–b)** WE: 1 h Sn@Cu, RE: Ag wire, CE: Li metal; scan range OCV to 0 V; scan rates of 10 mV s^{-1} and 1 mV s^{-1} for (a) and (b), respectively. **(c–f)** WE: 1 h Sn@Cu, RE: Li metal, CE: Li metal; scan range −0.5 V to OCV; scan rate of 10 mV s^{-1}. Panels (d) and (f) correspond to the same experiments as (c) and (e), respectively, with only four scans shown for clarity. Scans 50 and 100 are omitted in (c) for clarity but included in (d).

In Fig. S4a, b, only alloying and dealloying occur because the potential is restricted to above 0 V. In both cases, the current begins to decrease sharply at ~0.4 V, corresponding to the onset of alloying. As the scans proceed, a pronounced reduction peak gradually emerges at ~1.4 V at a scan rate of 10 mV s^{-1} and ~1.1 V at 1 mV s^{-1}. This peak may be associated with the continuous reduction of copper oxides, suggesting that repeated alloying and dealloying processes progressively damage the Sn coating and expose the underlying Cu surface to the electrolyte. However, the reduction capacity observed here is significantly larger than that typically reported for copper oxide reduction in Cu||Li cells, where the reduction current generally decays rapidly after the initial cycles. Further investigation is therefore required to confirm the origin of this reduction process.

In Fig. S4c–f, both electrodeposition and alloying occur because the potential is extended to −0.5 V. At later stages of cycling (approximately after scan number 10), a plateau around 0.8 V becomes apparent, which may be associated with alloying or SEI formation occurring on a cracked or partially exposed coating.

Figure S5 Voltage profiles and the identification of the transition between alloying and plating; stripping and dealloying.

The transitions between alloying and lithium plating during the negative current step, and between lithium stripping and dealloying during the positive current step, were identified from the voltage–time profiles using a slope-based analysis. The voltage traces were first smoothed using a Savitzky–Golay filter to reduce noise, and the absolute voltage slope (|dV/dt|) was calculated. A threshold separating plateau-like and sloping regions was defined from the distribution of |dV/dt| values using the 20th and 80th percentiles of each segment. The transition point was determined as the onset of a sustained change in slope magnitude relative to this threshold. Capacities associated with alloying, plating, stripping and dealloying were obtained by integrating the current over the corresponding time intervals. As shown in Fig S5, this method is good in identifying transition points before cycle 80.

Figure S6 Voltage profile of cycle 80 of a 1 h Sn@Cu||Li cell cycled at 0.5 mA cm^{-2} for 0.5 mAh cm^{-2}.

Determination of the transition from stripping to dealloying in our code has been discussed above, however, an upper voltage limit on dealloying is not set. For the voltage profile in Fig. S6 it determines every point above the inflection point to be dealloying despite a significant amount of time spent at 2.5 V. This results in graphs of the type shown in Fig. 9 having a resurgence of dealloying capacity after the point at which the cell has failed. There is no corresponding increase in the alloying capacity at these higher cycle numbers and so this parasitic reaction is clearly not dealloying. Therefore, in all graphs of this type, the region after cell failure should be ignored.

In samples which were aged for two months at room temperature more diffusion can occur resulting in a larger intermetallic compound layer. This results in differing behaviour in the breakdown of capacities when compared with a sample which is used days after being prepared. There is substantially more capacity coming from dealloying during the positive-current process, and more capacity from alloying in the negative-current process after 10 cycles. This increased alloying and dealloying character leads to the pulverisation of the sample as seen in samples limited to a discharge voltage of 3 V (i.e., fully de-lithiated), leading to coating failure after 60 cycles. Unlike freshly used samples there is no resurgence in the dealloying capacity and no stripping capacity peak leading to a trough at cycle 60 instead of a peak.

Figure S7 Decoupling of alloying and plating (left), dealloying and stripping (right) for aged 1-hr Sn@Cu||Li cell, cycled at 0.5 mA cm^{-2} with a capacity of 0.5 mAh cm^{-2}.

Calculation of of change over points between alloying and plating and stripping and dealloying in Fig. S8 was done using the procedure set out in Fig. S5. Lithium plating should only occur at voltages of 0 V or below which is clearly shown in cycle 30 above but the analysis works poorly for cycle 3. During early cycles, in aged samples, the peak associated with alloying is very broad (may also contain oxide reduction for aged samples) and this results in a brief plateau of the voltage above 0 V. This means that in the first few cycles, ~ <5, determination of the switch over point is substantially off. This also results in seemingly impossible alloying:dealloying ratios where more lithium is being dealloyed than alloyed. The alloying capacity calculated for the aged 1-hour sample during the first five cycles is actually mainly associated with SEI formation.

It is possible to avoid this error by using a simpler threshold-voltage analysis, for example assigning the voltage regions above −0.05 V (during lithiation) and above +0.2 V (during delithiation) vs. Li^+/Li to Sn alloying and dealloying, respectively, while regions below −0.05 V and below +0.2 V vs. Li^+/Li correspond to Li plating and stripping. However, this approach still presents issues in the early cycles.

Figure S8 *Voltage Profiles of 2 month aged Sn@Cu||Li cells for cycle 3 (right) and cycle 30 (left) cycled at 0.5 mA cm^{-2} with a capacity of 0.5 mAh cm^{-2}.*

Fig. S9 uses this more crude analysis with a fresh 1-hour Sn@Cu||Li using threshold voltages of –0.04 V to determine the alloying / plating boundary and 0.20 V to determine the stripping / dealloying boundary. Again this analysis works well for later cycles as there are no contributions from SEI formation, but in cycle 1 there is again a significant underestimation of the alloying due to SEI formation having not yet occurred, resulting in all potentials being shifted more negative for the negative-current processes. It is therefore very difficult to create an automated analysis method which works for every type of trace and so the behaviour of the first few cycle should be ignored.

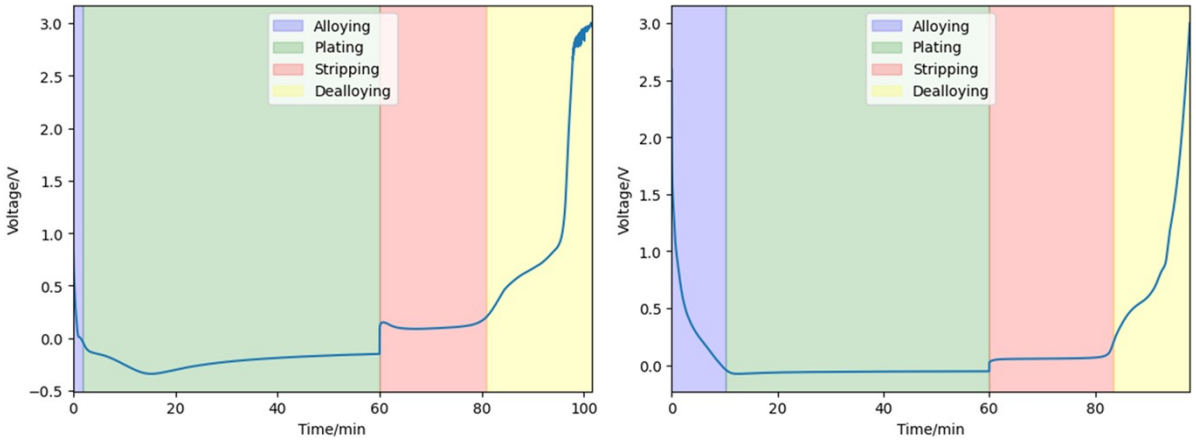

Figure S9 *Voltage traces of a fresh Sn@Cu||Li sample at cycle 1 (left) and cycle 30 (right). C charge and discharge rates, 0.5 mAh cm^{-2} capacity.*

In voltage limited Sn@Cu||Li cells it is clear in Fig. S10 that until at least cycle 80 there is almost no dealloying that occurs in any of the voltage limited cells despite significant dealloying being present in cells limited to 3 V. There is also limited alloying which only clearly occurs in the voltage limited samples up to cycle 10. These profiles demonstrate that enhanced cycling lifetime occurs because of the reduction in discharge potential and thus dealloying.

Comment []:

Figure S10 *Voltage profiles at cycles 1, 5, 10, 40, 80, and 180 for the 1-h Sn@Cu\Li cell cycled at 0.5 mA cm⁻² with a capacity of 0.5 mAh cm⁻² and upper cut-off voltages of 3 V (blue), 0.57 V (pink), 0.45 V (green), and 0.17 V (orange).*

The chemically pre-lithiated sample shows increased coulombic efficiency of ~15% per cycle for the first 50 cycles likely due to the increased plating and stripping character versus the standard coating. This increased performance suggests that pre-lithiation delays pulverisation of the coating due to fewer volume changes occurring during cycling.

Figure S11 *Discharge capacity and coulombic efficiency as a function of the cycle number for a 10-minute coating Sn@Cu||Li cell (orange) and a $Li_{4.4}$Sn@Cu||Li cell (blue) prepared by pressing Li metal against a Sn coated electrode for 1 hour and cycled at 0.5 mA cm^{-2} with a capcaity of 0.5 mAh cm^{-2}.*

Figure S12 *Breakdown of capacity contributions (using threshold method) for; a 10-minute Sn@Cu||Li cell in a) charge and b) discharge, and in a 10-minute Sn@Cu||Li cell where the electrode was pre-lithiated by pressing into Li metal overnight in LP57 in c) charge and d) discharge.*

By separating the capacities of a regular 10-minute coating and a chemically pre-lithiated 10-minute coating in Fig. S12 it is possible to see where the increased discharge capcaity comes from in the pre-lithiated sample in Fig. S11. Both samples have similar ratios of alloying to plating which is likely due to no voltage limits used resulting the dealloying of the pre-lithiated samples in the first cycle meaning they have to alloy very similarly in subsequent cycles. However, in the separation of the discharge capacities there is a larger percentage contribution from stripping in the pre-lithiated sample. This is likely due to differences in the first formation cycle resulting in a more preferable SEI allowing a higher amount of plating to occur in subsequent cycles.

Overpotential analysis

The overpotential of Li nucleation is a widely accepted metric for the analysis of Li electrodeposition. The typical analysis is done by subtracting the plateau voltage from the negative peak voltage. In tin-coated samples the voltage trace significantly changes over cycling (Fig. S13). This is due to contributions from many effects including lithium plating, lithium alloying and in the first couple of cycles SEI formation, all changing over time. By cycle 50 the voltage trace becomes very "copper-like", and calculation of the overpotential can be done simply by subtracting the plateau voltage from the negative peak voltage (Method 1), whereas during early cycles, e.g. cycles 5 and 10, a more complex analysis is required.

While the initial peak is potentially a result of the same phenomena, but the second peak and subsequent decrease in voltage do not plateau and continue to steadily decline over time. This makes determination of the plateau voltage difficult as the lower-voltage region between the peaks may not ever reach the plateau voltage due to this secondary peak and so any calculation of the overpotential for these cycles is inherently approximate (Method 2). The matter is further complicated in the very early cycles such as cycle 1 above where SEI formation is a significant factor affecting the voltage. This SEI formation results in the combination of all peaks into one much larger peak and a tail that steadily decreases in voltage. Calculation of the overpotential in these first few cycles is almost impossible from this, and any comparisons between samples likely have no meaningful connection to physical differences.

Figure S13 *Zoomed in voltage time profiles for charging half cycle of a 1 h Sn@Cu||Li half cell with a 0.17 V limit during discharge for cycles: 1 (top left), 5 (top right), 10 (bottom left) and 50 (bottom right). LP57 electrolyte, Charge rate = Discharge rate = 1C, 0.5 mAh cm^{-2} capacity.*

A possible method calculating a reasonable overpotential for all but the first cycle could be to take the first voltage as the peak voltage of nucleation of lithium on tin as this peak remains until late cycle numbers and take the plateau region as either a) the minimum voltage between the two peaks (cycles 5, 10 Fig. S1) or b) if only one peak is present (cycle 50 Fig. S13) taking the minimum voltage from the whole plateau region. This method has been compared to simply taking the overall minimum voltage as the peak and the final voltage during a cycle as the plateau voltage in Fig. S14 and shows that this analysis works

well for a Sn@Cu||Li sample limited to 0.17 V for the first 120 cycles, however, offers no improvement in the analysis of a Sn@Cu||Li sample limited to 3 V. It is clear from the voltage profiles shown in Fig. S14 below why this is the case.

Figure S14 *Voltage traces for the charging process of a 0.17 V discharge limited 1 h Sn@Cu||Li cell is shown for cycles a) 5 and b) 150, and for a 3.00 V discharge limited Sn@Cu||Li cell for cycles c) 5 and d) 30.*

The 0.17 V limited cell has the profile as shown in Fig. S14(a) for the first 120 cycles. After this point there are no more well-defined peaks and an overpotential cannot be calculated from this resulting in the fall of overpotential seen. For a cell limited to 3.00 V, however, the two peaks overlap close together in the early cycles which obscures the plateau in between the two peaks. This means that method of calculating the overpotential as set out in Fig. S14 is insufficient. Therefore, there is no method of calculating overpotential which can apply to all cycles in all types of cells which is further convoluted by the cycling procedure resulting in different overpotentials being obtained making it very difficult to create a meaningful comparison with bare copper current collectors in the literature. It is therefore necessary to use methods other than overpotential to determine the cause of improved performance from tin coatings.

Figure S15 *Overpotential has been calculated in 1 h Sn@Cu||Li cells with a 0.17 V discharge limit (yellow) and a 3.00 V limit (green) using method 1 (left) and method 2 (right).*

SEM imaging in Fig. S16 shows that it is possible to view the nucleation sites of lithium after repeated cycling if surface layer is scraped off. These are believed to be nucleation sites as they are circular in nature and have a sporadic density which aligns with the flower nature of the plated lithium as seen in Fig 3. The nucleation sites are potentially more metallic and electron conducting compared to the Sn@Cu surface which is likely to be covered by thicker insulating SEI and Sn oxide layer.

Fig S16 *SEM images showing nucleation sites of 10-minute Sn@Cu||Li cells after 40 cycles at 0.5 mA current for 0.5 mAh* cm^{-2} *capacity and scraped until Sn surface is visible.*

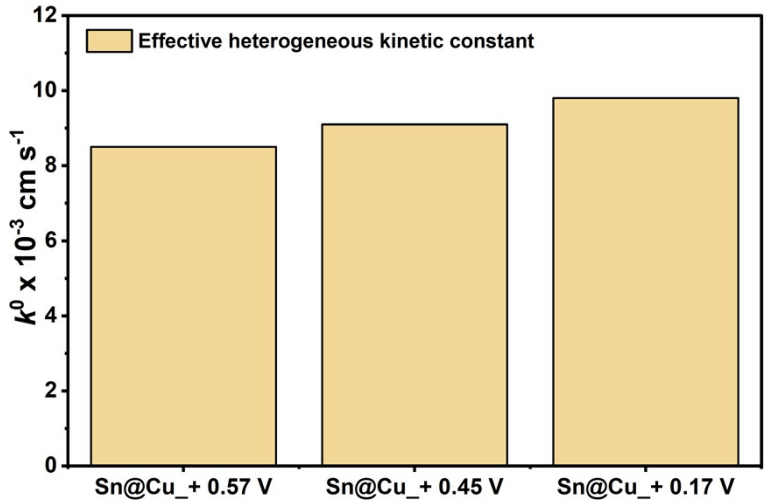

Fig S17 Bar diagram of the effective heterogeneous kinetics constant (k^0) values for Sn@Cu at + 0.57 V, + 0.45 V, + 0.17 V derived from fitting the experimental approach curves. Values of k^0 reported in units of x 10^{-3} cm s^{-1}.

Substrate	Conditions/ Potential	κ	k^0 X 10^{-3} cm/s
Cu	@ OCP	0.23	6.9
Sn@Cu	@ OCP	0.32	9.6
Sn@Cu	+ 0.57 V	0.28	8.4
Sn@Cu	+ 0.45 V	0.30	9.0
Sn@Cu	+ 0.17 V	0.35	10.5
Sn@Cu	+ 0.005 V	0.24	7.1
Second set			
Sn@Cu	+ 0.57 V	0.28	8.5
Sn@Cu	+ 0.45 V	0.30	9.0
Sn@Cu	+ 0.17 V	0.33	9.8

Table S3 Summary of the dimensionless heterogeneous rate constant parameter, κ and the corresponding effective heterogeneous rate constant k^0 (k^0 = □ D/a) that were extracted from the recorded approach curves using a diffusion coefficient for ferrocene of D = 1.5 x 10^{-5} cm^2 s^{-1} and a SECM tip radius is 5 x 10^{-4} cm.

Comparison with Cu||Li half-cells cycling

Non-coated Cu current collector sample was tested in two-electrode coin cells via galvanostatic cycling, the resulting voltage profile is shown in Fig. S18, where its performance was compared to the best performing Sn@Cu sample, pre-lithiated Sn@Cu with a cutoff voltage of 0.57V (presented in Fig.12 in the manuscript).

The bare Cu‖Li cell shows a cycling and CE trend similar to Sn@Cu when the stripping voltage is set to 3 V (effectively not restricted, Fig. 11in the manuscript). Although the initial stripping capacity of the bare Cu‖Li cell is significantly higher (potentially due to Sn alloy lithiation and Sn oxide reduction in Sn@Cu), it drops rapidly during the first 25 cycles, then stabilises for about 75 cycles before failure. While such fast degradation is typical for anode-free batteries (see ref. [1] in the manuscript), the subsequent stabilisation is unusual and may result from the presence of a large lithium reservoir.

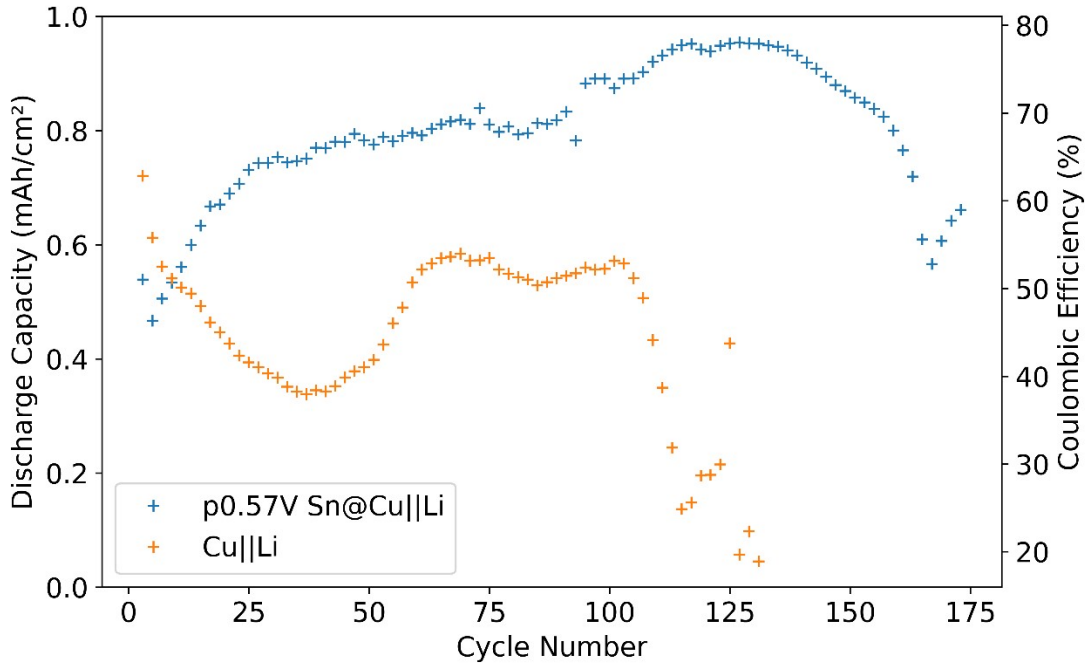

Fig S18 CE and stripping capacity as a function of cycle number for a Sn@Cu\|\|Li cell with an upper cut-off voltage of 0.57 V (blue) compared to a bare Cu\|\|Li cell. The Sn@Cu electrode exhibits enhanced cycling stability, higher CE, and improved capacity retention relative to the Cu counterpart, indicating more reversible lithium plating/stripping behaviour.